# Roughness of silicon nanowire sidewalls and room temperature photoluminescence

Vladimir A. Sivakov,[1,*,†] Felix Voigt,[1,2] Andreas Berger,[1,3] Gottfried Bauer,[2] and Silke H. Christiansen[1,4,‡]
[1]*Institute of Photonic Technology, Albert Einstein Str. 9, D-07745 Jena, Germany*
[2]*University of Oldenburg, Institute of Physics, Carl-von-Ossietzky-Straße 9-11, D-26129 Oldenburg, Germany*
[3]*Max Planck Institute of Microstructure Physics, Weinberg 2, D-06120 Halle (Saale), Germany*
[4]*Max Planck Institut für die Physik des Lichts, Günther Scharowsky Str. 1, D-91054 Erlangen, Germany*
(Received 19 March 2010; revised manuscript received 30 June 2010; published 27 September 2010)

Strong room temperature visible (red-orange) photoluminescence (PL) has been observed in silicon nanowires (SiNWs) that were realized by wet chemical etching of heavily (arsenic, As: $10^{20}$ $cm^{-3}$) and lowly doped (boron, B: $10^{15}$ $cm^{-3}$) single crystalline silicon (Si) wafers. Optical characterization of these SiNWs by PL combined with structural characterization by transmission and scanning electron microscopy strongly suggest that the visible PL at room temperature results from the rough SiNW sidewall structure that is composed of nanoscale features in which quantum confinement effects may occur.

DOI: 10.1103/PhysRevB.82.125446 PACS number(s): 78.55.Ap, 62.23.Hj, 68.37.Hk, 68.37.Og

## I. INTRODUCTION

Bulk silicon has a relatively small and indirect energy gap that leads to room temperature (RT) near band-edge luminescence at around 1.09 eV.[1–3] On the contrary, photoluminescence (PL) of nanoscale silicon structures such as porous silicon, nanowires, and quantum dots shows additional high-energy peaks in room temperature PL spectra[4] that are mediated by the nanoscale features. In the scientific literature few mechanisms have been thoroughly discussed as being responsible for the various PL features reported in porous silicon.[4–7] The first mechanism attributes the visible PL peaks to quantum size effects that can very well be probable in the filaments constituting the porous silicon.[8] A second mechanism relates additional peaks to a siloxenelike film supposedly covering the porous silicon surface.[9] The nonstable, varying PL observations in porous Si have been related to some kind of interface states located between the silicon and the siloxenelike surfaces.[10] A clear understanding of the PL of nanostructured Si would be highly appreciated for progressing thin-film Si nanostructure based solar cells or other photonic devices that could possibly be made out of this class of materials. The major hurdle in widely applying Si thin films for photovoltaic and photonic applications is its weak light absorption and emission in the visible wavelength regime that is caused by the indirect band gap of Si.[11–13] Nanostructured Si has already proven to enhance light absorption.[14] It is however not clear whether light is absorbed in the Si nanostructure itself or at defects at the large nanostructure surfaces.[15] The former would be desirable for using Si-based nanostructures in photonic applications since the utilization of the generated electron-hole pair could more easily be controlled. It was discussed whether Si nanostructures assume a quasidirect gap due to an increase in momentum uncertainty of the electron and hole wave functions. Hence, radiative recombination would drastically increase and therefore—which is more significant with respect to thin-film solar cells—also absorption of photons would become stronger. Unfortunately it became clear that silicon—even if nanostructured—conserves its indirect band-gap character, accompanied by rather slow phonon-assisted transitions.[16–18] However, absorption in one-dimensional structures, for example, silicon nanowires (SiNWs) is increased by other means. Due to the wavelength of incident light being larger than typical SiNW diameters, absorption is significantly enhanced with respect to bulk silicon.[19–22] In this work, we report morphological and optical studies on wet chemically etched lowly and heavily doped single crystalline silicon (c-Si) wafers containing SiNW structures.[23–27] We will discuss the changes in the PL spectra resulting from variations in doping level of etched SiNWs and the specifics of SiNW sidewall structures. The main aim of this work is to demonstrate the interrelation between optical (PL) phenomena and structural properties of the SiNWs, and to contribute to the clarification of the origin of RT visible PL in etched SiNWs. Furthermore, we demonstrate that SiNWs can show a strong RT light emission when starting with heavily doped wafers or a relatively lower PL when using lower doped wafers.

## II. EXPERIMENTAL SECTION

Lowly boron-doped (doping level: $10^{15}$ $cm^{-3}$; conductivity: 5–10 Ω cm) and heavily arsenic- (doping level: $10^{20}$ $cm^{-3}$; conductivity: <0.005 Ω cm) doped 100 mm (4 inch) diameter Si(111) c-Si wafers were used in this study. The silicon wafers were cleaned by rinsing in acetone for 2 min followed by an ethanol rinse for another 2 min. Native $SiO_2$ removal was carried out by a short dip in 40% hydrofluoric acid (HF) solution followed by a 2% HF rinse for 1 min. Finally, the samples were rinsed in de-ionized water and blow dried with nitrogen. This cleaning procedure yields hydrogen-terminated silicon surfaces (for a limited time of a few minutes[28,29]), which allowed for subsequent silver deposition on essentially oxide free-silicon wafer surfaces. Our chemical etching method to produce SiNWs is based on a two-step process, as was reported in our previous work.[30] In the first step, Ag nanoparticles were deposited on silicon wafer surfaces by immersing the wafers in aqueous solution of 0.02 M silver nitrate ($AgNO_3$) and 5 M HF in the volume ratio 1:1 (solution I) for 30 s. In the second step, silicon wafers covered with Ag nanoparticles were immersed in a

 ©2010 The American Physical Society

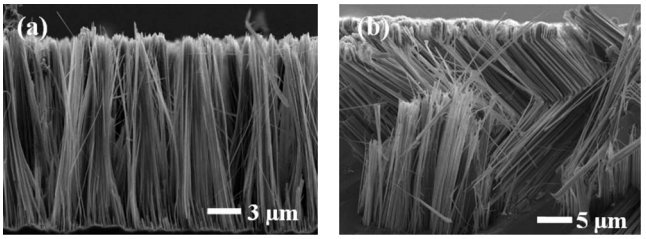


FIG. 1. Typical SEM cross section views of the (a) vertical and (b) zigzag SiNWs observed after wet chemical etching of (a) lowly boron- (5–10 Ω cm) and (b) heavily arsenic- (<0.005 Ω cm) doped Si(111) wafers.

second etching solution of 5 M HF and 30% $H_2O_2$ in the volume ratio 10:1 (solution II) in a teflon vessel for 60 min at room temperature. Finally, the surfaces obtained after the etching procedures with solutions I and II were rinsed several times in de-ionized water and dried at room temperature. The arrays were washed in a concentrated (65%) nitric acid ($HNO_3$) for 15 min to remove residual Ag nanoparticles from the SiNW surfaces. For comparison, a sample of porous silicon, prepared by electrochemical etching of a wafer following the procedure in Refs. 6 and 31 was investigated. For preparation a weakly boron-doped c-Si wafer with resistance of 20 Ω cm was used and a etch current of density 10 mA/cm$^2$ was applied for 20 min. Structural analysis of the etched SiNWs has been carried out by field emission scanning electron microscopy (JEOL JSM-6300F) and high-resolution transmission electron microscopy (HRTEM, FEI CM200/UT). The Fourier transform infrared (FTIR) spectrometer 670 coupled to the FTIR microscope 20 equipped with a mercury cadmium telluride detector (Varian, USA) was used for FTIR spectroscopy. FTIR spectra were recorded in reflective mode and in attenuated total reflection (ATR) mode. The ATR accessory (Varian) was based on a germanium prism. The spectrometer, the microscope, and the sample chamber were continually purged by dried air from air purifiers. Sixteen scans at 4 cm$^{-1}$ spectral resolution were collected to produce the resulting spectrum from 700 to 3000 cm$^{-1}$.

## III. RESULTS AND DISCUSSION

Wet chemically etched SiNWs are realized using single c-Si wafers of different doping levels. The wet chemical etching involves treatment of silicon surfaces with solutions I and II ($AgNO_3$, HF, and $H_2O_2$-based chemistries) as was specified in the experimental section. Depending on processing conditions, the SiNW morphologies differ with respect to starting wafer orientation and wafer doping type and level. Figure 1 shows scanning electron microscopy (SEM) micrographs of straight [Fig. 1(a)] as well as zigzag [Fig. 1(b)] SiNWs. Homogeneous SiNW morphologies are observed when using a comparably dense layer of silver nanoparticles as they form as a result of 30 s treatment in the $AgNO_3$/HF solution (solution I).[30]

The SiNWs in diameter varied from 30 to 200 nm with an average diameter of approximately 70 nm, as measured by

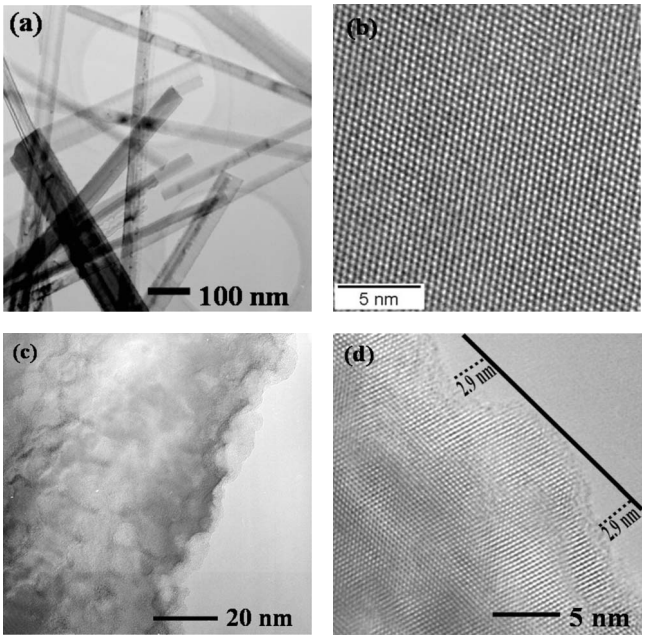


FIG. 2. TEM characterization of the rough SiNW surfaces (a) bright-field TEM image of wet-chemically etched SiNWs. The diameter distribution between 30 and 200 nm is clearly visible. The selected area in the HRTEM image (b) indicates that the SiNW is single crystalline all along its length. High-resolution TEM images (c) and (d) of the etched SiNW. The roughness is evident at the interface between the crystalline Si core and the amorphous native oxide shell. A peak to valley height of the sidewall roughness lies typically between 2.5 and 3.5 nm.

TEM [cf. Fig. 2(a)]. All SiNWs are single crystalline and are wrapped by a thin native silicon oxide layer as visible in the high-resolution TEM micrograph in Fig. 2(c) or Fig. 2(d). In contrast to the smooth surfaces of typical vapor-liquid-solid[32] grown, gold catalyzed SiNWs (Refs. 33 and 34) the surfaces of etched SiNWs are much rougher as shown in the TEM micrographs in Figs. 2(c) and 2(d). The average surface roughness of etched SiNWs was typically 2.5–3.5 nm measured from peak to valley. The formation of rough surfaces during the SiNW etching may be related to the silver nanoparticle enhanced local Si oxidation and subsequent oxide etching and further to migration of silver nanoparticles along the SiNW sidewalls during the etching process that was recently discussed by Qu *et al.*[35] The resulting arrays were vertically or oblique oriented and comprised single crystalline nanowires covering approximately 99% of the wafer area that is much higher than corresponded values by Hochbaum *et al.*[36]

PL was measured by a setup mainly based on a glass fiber and an optical multichannel analyzer (OMA). The setup is sketched in Fig. 3. Excitation light originating from an $Ar^+$ ion laser passes a line filter (F1, 488 nm) and a pin hole (PH) of 1.1 mm diameter before hitting the sample. The photon flux density of the excitation light at 488 nm wavelength at the place of the sample is $8.3\times10^{17}$ s$^{-1}$ cm$^{-2}$. PL is collected at a distance of 50 mm in backscattering direction deviating from direction of the incident beam by an angle of 25°. After passing a low pass filter (F2, 515 nm), the emitted

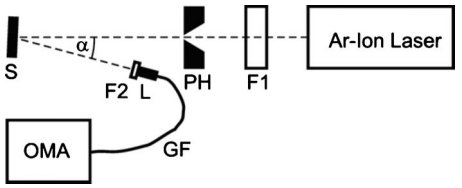


FIG. 3. Schematic representation of PL measurement setup. F1 is a line filter for 488 nm wavelength. PH is a pin hole of 1.1 mm in diameter, with a wedge angle of $\alpha=25°$. F2 is a low pass filter for a wavelength of 515 nm. $L$ is a lens for PL light collection with a focal length of $f=15.3$ mm. GF is an optical glass fiber. OMA is an optical multichannel analyzer.

light is coupled by a lens ($L$) into the glass fiber and transferred to the OMA, where the spectral PL intensity is measured by means of an InGaAs linear photodiode array with sensitivity up to 1.7 $\mu$m. The setup was calibrated by a tungsten band lamp of known temperature in order to facilitate the conversion from measured spectral response to PL photon flux distributions vs photon energy.

Room temperature PL being visible just by the naked eye was observed for wet chemically etched samples using Si wafers of various doping levels. However, the strongest visible PL being observed for wet chemically etched heavily arsenic-doped wafers. Figure 4(a) shows a PL spectrum for a heavily arsenic-doped wafer recorded with the setup shown in Fig. 3. The light emission in the red-orange wavelength regime is visible on the digital photos, shown in Fig. 4(c). Here, the sample was illuminated by day light [Fig. 4(b)] and by a nitrogen laser with a wavelength of 337 nm [Fig. 4(c)]. The exposure time was 2 s for both digital images. The strong visible PL reminds both of the well-known PL of porous silicon[4] and of the PL of silicon nanocrystals (SiNCs).[37]

To clarify which are the states that are responsible for the visible PL, further experiments were performed. A key experiment for the exploration of the origin of the PL is the investigation of samples before and after treatment with 2.5% HF in water. Dilute HF removes $SiO_x$ compounds from the Si sample surfaces and passivates these surfaces for several minutes from oxidation by inducing a hydrogen termination of dangling bonds at the Si surfaces. In Fig. 5(a) the effect of HF treatment on heavily arsenic and weakly boron-doped chemically etched samples is presented. The HF treatment induces a redshift of the maximum in the PL spectrum as shown in Table I. For direct comparison, Table I shows PL maxima or $E_{max}$ (maximum photon energy) of different samples before and after HF treatment. We have selected for this comparison two identical heavily arsenic-doped samples and one lowly boron-doped sample as obtained from wet chemical wafer etching. Moreover we have used a porous silicon[31] sample as reference formed as was before specified in the experimental section. These $E_{max}$ values were obtained after application of raw data smoothening using a ten-point moving average smoothening algorithm. The experimental setup concerning excitation and detection in all measurements remained the same, hence PL yields of SiNW samples and the porous sample can be compared. The absorption length of c-Si at 488 nm amounts to $1/\alpha=0.8$ $\mu$m [20] and absorption in nanostructured Si is even higher[20] therefore in the etched samples of typically several micrometers thickness we can assume almost all incident photons to be absorbed. In summary we can conclude that the strongest PL of the SiNW samples is almost as efficient as the PL of the porous Si sample, only about a factor of 2 lower.

Further, Fig. 6 shows the evolution of PL measured in air after HF treatment. During reoxidation the PL signal recovers and nearly reaches its initial form (before HF treatment) after 40 min. Interestingly, substantial PL remains after HF treatment of the SiNW sample surfaces.

Consequently, the reason for room temperature PL cannot be attributed entirely to $SiO_x$-based interface states. We conclude, from the comparison of PL measurements in Table I that the observed PL of the as-prepared samples can partly be associated to the presence of $SiO_x$-based interface states. This finding is supported by TEM investigations that show a thin silicon oxide layer on the SiNWs in the micrographs in Figs. 2(c) and 2(d). The remaining room temperature PL after HF treatment cannot be attributed to $SiO_x$-based interface states but needs to have a different origin. The PL obtained for the porous Si sample prepared by electrochemical wafer etching is, however, not similar to the one obtained for our wet chemically etched samples. This can be seen following the PL spectra in Fig. 5(b) of the porous Si sample before and after HF treatment and the derived maximum PL peaks included in Table I. It is obvious that the PL in case of the porous Si sample almost entirely vanishes after HF treatment. Hence, we conclude that the origin of room temperature PL of wet chemically etched samples is not solely due to $SiO_x$-based interface states in contrary to PL of the electrochemically etched porous Si sample.

FTIR studies on the silicon nanowire surfaces, before and after hydrofluoric acid treatment, reveal information about the surface structure of the silicon nanowire that can be useful for the explanation of optical effects observed in the PL spectra of SiNWs. The FTIR spectra taken between 500 and 3000 $cm^{-1}$ of freshly prepared and HF treated SiNWs formed by wet chemical etching of heavily doped Si(111) wafers are shown in Fig. 7.

These spectra show that the HF treated SiNW ensembles contain well-defined $Si\text{-}H_x$ absorption bands at around 910 and 2086–2138 $cm^{-1}$.[38–40] These absorption bands are re-

TABLE I. PL maxima positions before and after HF treatment.

| | Heavily doped SiNWs1 (eV) | Heavily doped SiNWs2 (eV) | Lowly doped SiNWs (eV) | Porous Si (eV) |
|---|---|---|---|---|
| $E_{max}$ before HF | 1.54 | 1.52 | 1.48 | 1.75 |
| $E_{max}$ after HF | 1.43 | 1.45 | 1.33 | Low res. |

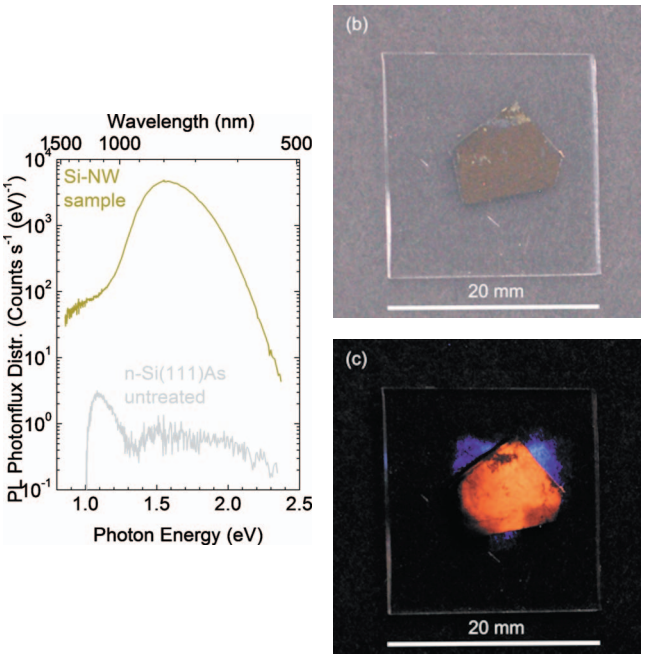


FIG. 4. (Color) Room temperature visible PL of treated and untreated (as reference) heavily doped *n*-type arsenic-doped Si(111) (<0.005 Ω cm; $10^{20}$ cm$^{-3}$). (a) PL spectrum obtained with irradiation at a wavelength of 488 nm for treated and untreated heavy-doped silicon wafer. (b) Digital micrograph of the sample mounted on a corning 7059 glass surface irradiated by day light. (c) Sample irradiated by a nitrogen laser at a wavelength of 337 nm. Visible blue emission next to the orange emission from the SiNW sample is due to fluorescence of the glass substrate.

lated to Si-$H_x$ groups adsorbed at the SiNW surfaces.[41] Compared to the FTIR spectra of freshly prepared SiNW ensembles, the most relevant differences appear close to frequencies related to the Si-O bond between 800 and 1200 cm$^{-1}$. The signals at 1165 and 1240 cm$^{-1}$ correspond to the stretching and symmetrical and antisymmetrical vibrational modes of the Si-O-Si bridges in $SiO_x$.[40,42] These

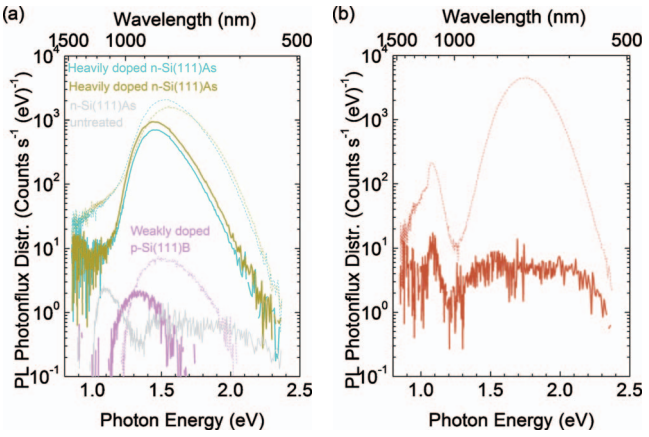


FIG. 5. (Color) (a) PL spectra of the etched lowly and heavily doped SiNWs before (dashed line) and after (solid line) treatment with 2.5% HF for 3 min. (b) PL spectra of porous Si before (dashed line) and after (solid line) treatment with 2.5% HF for 3 min, serving as a reference sample.

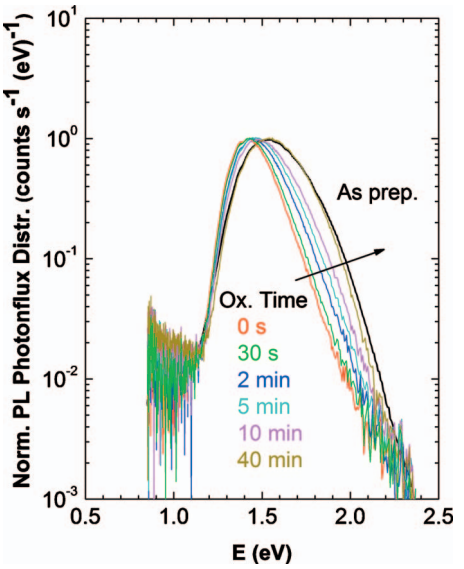


FIG. 6. (Color) Normalized PL spectra of the wet chemically etched heavily doped c-Si before (black line), after (red line) treatment with 2.5% HF for 3 min and during reoxidation under air atmosphere.

modes appear only in porous Si that contains some degree of oxidation at the large surface area. FTIR studies of the SiNWs, before and after HF treatments, reveal information on the adsorption at the large SiNW surfaces. According FTIR results the blueshift in PL spectra during reoxidation in Fig. 6 can be associated with the growth of native oxide layers on the silicon nanowires surfaces that also was specified in the TEM micrographs as shown in Fig. 2, where a 2–3 nm thick native oxide layer is clearly visible in as-prepared SiNWs' surfaces.

The vast majority of interpretations of the origin of visible PL in Si are related to quantum confinement in nanocrystalline Si,[4] to the presence of oxygen in $SiO_x$ surface states and to the formation of siloxenes and their derivates.[43–45] According to our PL and TEM results carried out for wet

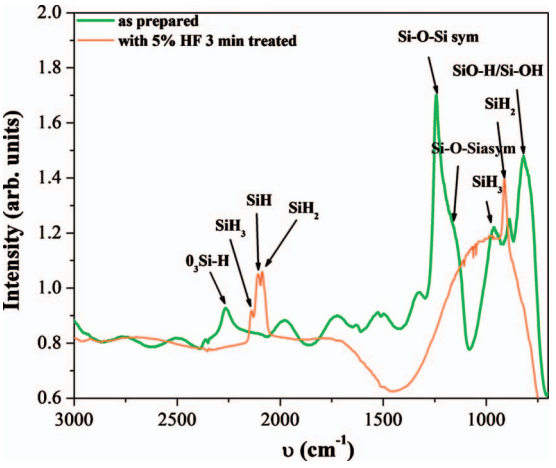


FIG. 7. (Color) FTIR absorption spectra of freshly etched heavily doped *n*-Si(111)As wafer before (green) and after HF (red) treatments.

chemically etched SiNWs the quantum confinement interpretation appears to be the most probable interpretation of the room temperature visible PL for our samples. We propose for our SiNWs that the remaining PL after HF treatment is related to nanoscale periodically rough sidewalls. According to Refs. 18 and 46 the SiNC diameters $d$ (nm) can be calculated from the PL peak energies $E$ (eV) using the relation

$$E = E_0 + 3\,.\,73/d^{1.39},$$

where $E_0 = 1.12$ eV is the room temperature band gap of bulk c-Si.

For the interpretation of our PL measurements an average energy $E_{\mathrm{SiNW}} = 1.40$ eV of the HF treated SiNWs is assumed. The deviation of 0.28 eV from the bulk c-Si energy $E_{\mathrm{bulk}}$ corresponds to nanocrystal diameters $d = 6.4$ nm. This agrees well with the dimensions of the periodically nanostructured rough sidewalls of the SiNWs. So far, it is not clear whether the nanostructures at the rough SiNW sidewalls are (i) localized nanocrystal-like features surrounded by oxide shells or (ii) semilocalized Si structures, which are still connected to the SiNW core by crystalline Si material. In case (i) theory of quantum confinement as known for SiNCs (Ref. 18) can be directly applied. In case (ii) the explanation of band-gap widening due to quantum confinement is not straight forward. A confined electron-hole pair could easily diffuse into the bulk of the SiNW, thereby loosing its confinement-related surplus energy. One would therefore expect PL at the band edge of c-Si to dominate in this case. Band-gap widening is only explainable, here, if one of the charge carriers, e.g., the hole, is trapped at the SiNW surface. Consequently, the other carrier would experience confinement. Confinement surplus energy in this case has to exceed the trapping energy of the hole (~50 meV necessary at RT) and the exciton binding energy (~19 meV for c-Si). Detailed experimental investigations, whether case (i) or (ii) is valid are still lacking and theoretical calculations of confinement energies in case (ii) yet have to be performed to the best of our knowledge. Nevertheless, trapping of holes at the $\mathrm{Si}/\mathrm{SiO}_x$ interface is known to occur[47,48] and the variety of available crystallographic planes at the rough SiNW surfaces make the trapping of holes at the $\mathrm{Si}/\mathrm{SiO}_x$ interface for SiNWs even more likely than for wafers with low index plane surfaces.

Another estimation suggested by Matsumoto *et al.*[49] derives the band-gap energy $E_g$ (eV) of Si nanocrystals according to

$$E_g = 1.06 + 2.05(1/L)^{1.6}$$

with $L$ (nm) being the nanocrystal diameter.

The roughness of the SiNW sidewalls shows peak-to-valley heights between 2.5 and 3.3 nm as shown in Fig. 2 that according to Matsumoto *et al.*[49] nanostructures of that size can cause band-gap energy shifts between 1.35 and 1.5 eV. The nanocrystalline Si investigated by Matsumoto *et al.*[49] was composed of SiNCs but in addition consisted in remains of amorphous Si and voids. An elucidating experiment with respect to the relationship of optical band gap and Si nanocrystal size was performed by Ledoux *et al.*[37,46] They used a setup in ultrahigh vacuum to produce SiNCs with a narrow size distribution (full width at half maximum around 1 nm or smaller) as determined by a time-of-flight mass spectrometer measuring directly in the deposition chamber. The optical band gap of their Si nanocrystals was measured using PL by taking the position of the maximum PL yield. Brüggemann[50] shows that the maximum of PL photon current of c-Si is located within $\pm 0.1$ eV precision around 1.1 eV, which is the room temperature band gap of c-Si (see Fig. 3 in Ref. 50). With respect to our rough SiNW surfaces we need to keep in mind that the nanocrystal-like structures are different in shape from ideally spherical SiNCs. Therefore, a difference in PL maximum position of spherical Si nanocrystals and periodic SiNW sidewall roughness are expected. It is probable that a spherical Si nanocrystal of approximately 6 nm in diameter will emit PL at an energy similar to the one of periodic sidewall structures of half that size, i.e., with approximately 3 nm periodic wavelength. Based on knowledge from porous Si investigations, the origin of visible PL in wet chemically etched SiNWs can be interpreted as a quantum confinement effect that originates from the periodically rough SiNW sidewall structures.

## IV. CONCLUSIONS

We have demonstrated that lowly and heavily doped SiNWs from wet chemical etching of single crystalline silicon wafers can strongly emit visible photoluminescence at room temperature. This behavior has been related to quantum confinement effects due to periodic nanoscale roughness of the SiNW sidewalls. Due to the etching procedure of the c-Si wafers and formation of nanostructures the silicon band gap was appreciably widened between 1.45 and 1.6eV.

## ACKNOWLEDGMENTS

The authors are gratefully acknowledged to H. Köbe and A. Dellith (Institute of Photonic Technology, Jena/Germany) for the scanning electron microscopy investigations and to S. Hopfe (Max-Planck-Institute of Microstructure Physics, Halle/Germany) for the preparation of the TEM samples. The support by FTIR measurements by Ch. Krafft (Institute of Photonic Technology, Jena/Germany) is acknowledged. Furthermore, we thank S. Knabe (University of Oldenburg, Oldenburg/Germany) for help in calibrating the PL setup and Stephan Schweizer for the preparation of the sample of porous silicon. V. Gerliz is gratefully acknowledged for measuring the PL during reoxidation of one of the samples. The authors gratefully acknowledge financial support by European Commission in part the European Project in the framework of FP7, "ROD-SOL" as well as by the Max-Planck-Society in the framework of the "NANOSTRESS" project.

*Author to whom correspondence should be addressed.
†vladimir.sivakov@ipht-jena.de
‡FAX: +49 (0) 3641/206-499; sechrist@mpi-halle.mpg.de

[1] J. R. Haynes and W. C. Westphal, Phys. Rev. **101**, 1676 (1956).
[2] W. Michaelis and M. H. Pilkuhn, Phys. Status Solidi **36**, 311 (1969).
[3] L. T. Canham, J. Phys. Chem. Solids **47**, 363 (1986).
[4] L. T. Canham, Appl. Phys. Lett. **57**, 1046 (1990).
[5] R. Tsu, H. Shen, and M. Dutta, Appl. Phys. Lett. **60**, 112 (1992).
[6] V. Lehmann and U. Gösele, Appl. Phys. Lett. **58**, 856 (1991).
[7] W. L. Wilson and T. Weidmann, J. Phys. Chem. **95**, 4568 (1991).
[8] G. C. John and V. A. Singh, Phys. Rev. B **50**, 5329 (1994).
[9] M. Koós, I. Pócsik, and E. B. Vázsonyi, Appl. Phys. Lett. **62**, 1797 (1993).
[10] H.-J. Lee, Y. H. Seo, D. H. Oh, K. S. Nahn, Y. B. Hahn, I. C. Jeon, E. K. Suh, Y. H. Lee, and H. J. Lee, J. Appl. Phys. **75**, 8060 (1994).
[11] W. R. Runyan, *Technology Semiconductor Silicon* (McGraw-Hill Book, New York, 1966).
[12] A. A. Wolfson and V. K. Subashiev, Fiz. Tekh. Poluprovodn. **1**, 397 (1967) (in Russian).
[13] G. G. Macfarlane, T. P. McLean, J. E. Quarrington, and V. Roberts, J. Phys. Chem. Solids **8**, 388 (1959).
[14] S. Bandiera, D. Jacob, T. Muller, F. Marquier, M. Laroche, and J.-J. Greffet, Appl. Phys. Lett. **93**, 193103 (2008).
[15] A. T. Fiory and N. M. Ravindra, J. Electron. Mater. **32**, 1043 (2003).
[16] O. Guillois, N. Herlin-Boime, C. Reynaud, G. Ledoux, and F. Huisken, J. Appl. Phys. **95**, 3677 (2004).
[17] C. Delerue, G. Allan, and M. Lannoo, Phys. Rev. B **64**, 193402 (2001).
[18] C. Delerue, G. Allan, and M. Lannoo, Phys. Rev. B **48**, 11024 (1993).
[19] L. Hu and G. Chen, Nano Lett. **7**, 3249 (2007).
[20] L. Tsakalakos, J. Balch, J. Fronheiser, M. Y. Shih, S. F. LeBoeuf, M. Pietrzykowski, P. J. Codella, B. A. Korevaar, O. Sulima, J. Rand, A. Davuluru, and U. Rapol, J. Nanophotonics **1**, 013552 (2007); M. A. Green and M. Keevers, Prog. Photovoltaics **3**, 189 (1995).
[21] Th. Stelzner, M. Pietsch, G. Andra, F. Falk, E. Ose, and S. H. Christiansen, Nanotechnology **19**, 295203 (2008).
[22] V. Sivakov, G. Andrä, A. Gawlik, A. Berger, J. Plentz, F. Falk, and S. H. Christiansen, Nano Lett. **9**, 1549 (2009).
[23] K. Q. Peng, Y. J. Yan, S. P. Gao, and J. Zhu, Adv. Mater. **14**, 1164 (2002).
[24] Z. Huang, X. Zhang, M. Reiche, L. Liu, W. Lee, T. Shimizu, S. Senz, and U. Gösele, Nano Lett. **8**, 3046 (2008).
[25] K. Q. Peng, Y. Wu, H. Fang, X. Y. Zhong, Y. Xu, and J. Zhu, Angew. Chem. **117**, 2797 (2005).
[26] A. I. Hochbaum, R. Chen, R. Diaz Delgado, W. Liang, E. C. Garnett, M. Najarian, A. Majumdar, and P. Yang, Nature (London) **451**, 163 (2008).
[27] C.-Y. Chen, C.-S. Wu, C.-J. Chou, and T.-J. Yen, Adv. Mater. **20**, 3811 (2008).
[28] D. B. Fenner, D. K. Biegelsen, and R. D. Bringans, J. Appl. Phys. **66**, 419 (1989).
[29] T. Takahagi, I. Nagai, A. Ishitani, H. Kuroda, and Y. Nagasawa, J. Appl. Phys. **64**, 3516 (1988).
[30] V. A. Sivakov, G. Brönstrup, B. Pecz, A. Berger, G. Z. Radnoczi, M. Krause, and S. H. J. Christiansen, J. Phys. Chem. C **114**, 3798 (2010).
[31] A. Uhlir, Bell Syst. Tech. J. **35**, 333 (1956).
[32] R. S. Wagner and W. C. Ellis, Appl. Phys. Lett. **4**, 89 (1964).
[33] V. Sivakov, F. Heyroth, F. Falk, G. Andrä, and S. H. Christiansen, J. Cryst. Growth **300**, 288 (2007).
[34] W. Lu and C. M. Lieber, J. Phys. D **39**, R387 (2006).
[35] Y. Qu, L. Liao, Y. Li, H. Zhang, Y. Huang, and X. Duan, Nano Lett. **9**, 4539 (2009).
[36] A. I. Hochbaum, D. Gargas, Y.-J. Hwang, and P. Yang, Nano Lett. **9**, 3550 (2009).
[37] G. Ledoux, J. Gong, F. Huisken, O. Guillois, and C. Reynaud, Appl. Phys. Lett. **80**, 4834 (2002).
[38] K. W. Cheah, T. Chan, W. L. Lee, D. Teng, W. H. Zheng, and Q. M. Wang, Appl. Phys. Lett. **63**, 3464 (1993).
[39] F. Ruiz, C. Vazquez-Lopez, J. Gonzalez-Hernandez, D.-D. Allred, G. Romero-Paredes, R. Pena-Sierra, and G. Torres-Delgado, J. Vac. Sci. Technol. A **12**, 2565 (1994).
[40] R. R. Koropecki and R. Arce, J. Appl. Phys. **60**, 1802 (1986).
[41] M. A. Vasquez-A, G. A. Rodriguez, G. Garcia-Salgado, G. Romero-Parades, and R. Pena-Sierra, Rev. Mex. Fis. **53**, 431 (2007).
[42] H. Yorikawa and S. Muramatsu, J. Lumin. **87-89**, 423 (2000).
[43] M. S. Brandt, H. D. Fuchs, M. Stutzmann, J. Weber, and M. Cadona, Solid State Commun. **81**, 307 (1992).
[44] H. D. Fuchs, M. Stutzmann, M. S. Brandt, M. Rosenbauer, J. Weber, and M. Cardona, Phys. Scr. **T45**, 309 (1992).
[45] P. Deák, M. Rosenbauer, M. Stutzmann, J. Weber, and M. S. Brandt, Phys. Rev. Lett. **69**, 2531 (1992).
[46] G. Ledoux, O. Guillois, D. Porterat, C. Reynaud, F. Huisken, B. Kohn, and V. Paillard, Phys. Rev. B **62**, 15942 (2000).
[47] R. J. Powell, J. Appl. Phys. **46**, 4557 (1975).
[48] X. Yuan, Y. Shi, S. Gu, J. Zhu, Y. Zheng, K. Saito, H. Ishikuro, and T. Hiramoto, Physica E **8**, 189 (2000).
[49] T. Matsumoto, J.-I. Suzuki, M. Ohnuma, Y. Kanemitsu, and Y. Masumoto, Phys. Rev. B **63**, 195322 (2001).
[50] R. Brüggemann, Philos. Mag. **89**, 2519 (2009).